 CMES, vol.83, no.1, pp.73-96, 2012

A Physically Meaningful Level Set Method for Topology Optimization of Structures

Zhen Luo[1,2], **Nong Zhang**[1,3] **and Yu Wang**[1]

Abstract: This paper aims to present a physically meaningful level set method for shape and topology optimization of structures. Compared to the conventional level set method which represents the design boundary as the zero level set, in this study the boundary is embedded into non-zero constant level sets of the level set function, to implicitly implement shape fidelity and topology changes in time via the propagation of the discrete level set function. A point-wise nodal density field, non-negative and value-bounded, is used to parameterize the level set function via the compactly supported radial basis functions (CSRBFs) at a uniformly defined set of knots. The set of densities are used to interpolate practical material properties in finite element approximation via the standard Lagrangian shape function. CSRBFs knots are supposed to be consistent with finite element nodes only for the sake of numerical simplicity. By doing so, the discrete values of the level set function are assigned with practical material properties via the physically meaningful interpolation. The original more difficult shape and topology optimization of the Hamilton-Jacobi partial differential equations (PDEs) is transformed to a relatively easier size optimization of the nodal densities, to which more efficient optimization algorithms can be directly applied. In this way, the dynamic motion of the design boundary is just a question of transporting the discrete level set function until the optimal criteria of the structure is satisfied. Two widely studied examples are applied to demonstrate the effectiveness of the proposed method.

Keywords: Topology optimization; level set method; compactly supported radial basis functions (CSRBFs); nodal density interpolation

[1] School of Electrical, Mechanical and Mechatronic Systems, The University of Technology, Sydney, NSW 2007, Australia

[2] State Key Lab. of Digital Manufacturing Equipment & Technology, Huazhong University of Science & Technology, Wuhan, Hubei 430074, China

[3] Corresponding Author. Tel: +61-2-9514 2662; Fax: +61-2-9514 2655. E-mail address: nong.zhang@uts.edu.au

1 Introduction

Structural topology optimization has experienced considerable development over the past with a number of applications in a broad range of fields [Bendsøe and Sigmund (2003)]. Topology optimization actually consists of an iterative numerical process to determine the best layout of a given amount of material in the extended reference domain subjecting to supports and loads until a prescribed design objective is extremized under specific constraints. Several typical methods have been developed in the past two decades, including the homogenization method [Bendsøe and Kikuchi (1988)], the SIMP method [Zhou and Rozvany (1991); Bendsøe and Sigmund (1999)], and the level-set based method [Sethian and Wiegman (2000); Wang, Wang and Guo (2003); Allaire, Jouve and Toader (2004)]. Particularly, the SIMP approach has experienced much popularity due to its conceptual simplicity and numerical easiness.

Level set method [Osher and Sethia (1988); Sethian (1999); Osher and Fedkiw (2002)] has attracted much attention as an emerging approach to structural shape and topology optimization since the research of Sethian and Wiegmann (2000). After that, a number of level set methods have been developed for shape and topology optimization problems based on standard level set model [e.g. Osher and Santosa (2001); Wang, Wang and Guo (2003); Allaire, Jouve and Toader (2004); Yamasaki, Nishiwaki, Yamada, Izui, and Yoshimura (2010a); Yamada, Izui, Nishiwaki, and Takezawa (2011b)]. Shape derivative analysis [Sokolowski and Zolesio (1992)] is usually used in finding the velocity field to enable the dynamics of the design boundary. As a relatively new approach to structural optimization, the level set method can offer flexibilities with shape fidelity and topological changes, maintaining concise interface with smooth state, weak solutions and entropy limits. However, numerical difficulties relevant to the solution of the complicated Hamilton-Jacobi PDEs limit the further application of the level set methods to shape and topology optimization. To overcome the difficulties, some alternative level set methods are developed without solving these complicate PDEs [e.g. Belytschko, Xiao and Parimi (2003); Haber (2004); Luo, Tong and Wang (2008); Luo, Tong, Luo and Wang (2009)].

Radial basis functions (RBFs) have been introduced for scattered data interpolation problems in multivariate Euclidean space [Buhmann (2004)]. With RBFs, we can achieve the strictly positive definiteness of the interpolation matrix, and the unique existence of expansion coefficients for the interpolation problem. Particularly, the compactly supported radial basis functions (CSRBFs) [Wendland (2005)] have experienced popularity in multivariate interpolations for large scale scattered data. One advantage is giving rise to the positive definiteness and sparseness of the interpolation matrices. A further advantage is that the interpolant can naturally inherit

the continuity of its basis function. That is, the continuity of the interpolation is determined by the continuities of the shape functions and their partial derivatives. Wendland (2005) constructed a family of CSRBFs possessing the lowest degree with prescribed order of smoothness.

However, in level set methods, the level set function is only a mathematically defined scalar function [Sethian (1999)], which doesn't have any definite physical meanings connected to practical material properties (e.g. material density and elastic modulus). Actually, in standard level set methods, the values of the discrete level set function are the design variables to update boundary shapes and structural topologies. The level set function is only required to satisfy the Lipschitz continuity [Osher and Sethian (1988)], which is an enhanced continuity condition to bind the first-order derivatives to ensure the existence and uniqueness of the Hamilton-Jacobi PDEs solutions. In this case many scalar functions can be acted as the level set function, only if the continuity condition is satisfied. This will provide opportunities in constructing new discrete level set functions according to physically meaningful quantities for mechanics problems, such as material densities, elasticity modulus, strain or strain energy densities. Hence, one motivation of this paper is to make the level set function own definite physical meanings.

The nodal density-based interpolation schemes have been successfully applied in topology optimization [e.g. Kang and Wang (2011,2012)]. A physically meaningful nodal density interpolation should satisfy some basic requirements, such as $0<\rho \leq 1$ [Sigmund (2001)]. In this study, since the nodal density field for level set function interpolation is supposed to be non-negative and range-bounded, the design boundary cannot be defined at the zero level set compared to most conventional level set methods. Instead, the design boundary will be embedded into a set of non-zero constant level sets rather than the zero level set of the level set function., similar to the definition of the boundary in the piecewise constant level set method [Tai and Li (2007); Luo, Tong, Luo and Wang (2009)]. The constant level set where the design boundary is located can be numerically determined in terms of the lower and upper bounds of the discrete level set function during each step. In this method, the density field will be used as expansion coefficients to construct the discrete level set surface. It can converge to the regularized lower and upper bounds (0 and 1), and it is unnecessary to take any additional scheme to penalize the intermediate densities [Bendsøe and Sigmund (2003)]. Most of the above research works for topology optimization are based on finite element methods. It is noted that meshless methods can also be applied to topology optimization of structures, such as [Li and Atluri (2008); Zheng, Long, Xiong and Li (2008); Du, Luo, Tian, and Chen (2009)].

Hence, this work presents a new level set method for structural shape and topology

optimization based on the interpolation of point-wise nodal densities and CSRBFs on a set of scattered data. One attempt of this research is to let the level set function have definite physical meanings. The discrete level set function can be reconstructed in terms of the nodal point densities scattered in the design domain. The practical material properties can be constructed in terms of the density field and the solid-state material properties.

2 Nodal density-based level set parameterization

This Section focuses on a material density-based level set parameterization using CSRBFs.

2.1 Level set-based implicit free boundary representation

In this level set method, the interface is embedded into a higher-dimensional level set surface as a set of constant level-sets (e.g. 2D boundary to 3D surface), compared to the zero level set in the standard level set method [Osher and Sethian (1988); Sethian (1999)]. To enable the dynamic motion, introducing the pseudo-time t into the level set function leads to the following first-order 'Hamilton-Jacobi' PDE by differentiating it on both sides with respect to t:

$$\frac{\partial \Phi(\mathbf{x},t)}{\partial t} + \mathrm{v_n}\,|\nabla\Phi| = 0,\ \Phi(\mathbf{x},0) = \Phi_0(\mathbf{x}) \tag{1}$$

The normal velocity is expressed as follows:

$$\mathrm{v_n} = \mathrm{v}\cdot\mathrm{n} = \mathrm{v}\cdot\frac{\nabla\Phi}{|\nabla\Phi|} = \frac{d\mathbf{x}}{dt}\frac{\nabla\Phi}{\sqrt{\nabla\Phi\cdot\nabla\Phi}} \tag{2}$$

Hence, moving boundary $\Gamma = \{\mathbf{x}\,|\Phi(\mathbf{x}) = \mathrm{C}\}$ along norm al direction $\mathrm{n} = \nabla\Phi/|\nabla\Phi|$ is equivalent to transporting Φ by solving the Hamilton-Jacobi PDE with explicit time-marching schemes [Wang, Wang and Guo (2003); Allaire, Jouve and Toader (2004)] on a fixed Eulerian rectilinear grids. The velocity field is generally determined using the shape derivative analysis [Sokolowski and Zolesio (1992)]. As mentioned above, numerical difficulties in solving the Hamilton-Jacobi PDEs limit the further application of the level set method to topology optimization.

2.2 Parameterization using material density field and CSRBFs

The radial basis function [Buhmann (2004)] benefits the interpolation in several aspects, e.g. it is irrespective of the geometry of the knots, applicable to any dimensions, differentiable and relevant to elliptic differential operators and etc. The globally supported RBFs can ensure a higher-level accuracy of the interpolation but

it leads to a fully dense matrix poorly conditioned, which restricts their practical applications to large-scale topology optimization. However, the CSRBFs [Wendland (2005)] can reduce the computational expense, and provide a reasonable balance between the accuracy and computational effort for the interpolation.

2.2.1 CSRBFs

Here, the CSRBFs with 2k continuity such as C2, C4 and C6 functions [Wendland (1995)] are adopted to interpolate the level set function with desired smoothness and completeness. For a typical Wendland function with C4 continuity are given as follows:

$$\Theta(r(x,y)) = \{\max(0,(1-r(x,y)))\}^6 (35r^2(x,y)+18r(x,y)+3) \tag{3}$$

and its first order derivatives have the following forms

$$\frac{\partial \Theta(r(x,y))}{\partial x} = \frac{\partial \Theta}{\partial r}\frac{\partial r}{\partial x} = \{\max(0,(1-r(x,y)))\}^5 (-280r^2(x,y)-56r(x,y))\frac{\partial r}{\partial x} \tag{4}$$

$$\frac{\partial \Theta(r(x,y))}{\partial y} = \frac{\partial \Theta}{\partial r}\frac{\partial r}{\partial y} = \{\max(0,(1-r(x,y)))\}^5 (-280r^2(x,y)-56r(x,y))\frac{\partial r}{\partial y} \tag{5}$$

where the radius of support is given in a 2-D Euclidean space as

$$r = \frac{d_I}{d_{mI}} = \frac{\sqrt{(x-x_i)^2+(y-y_i)^2}}{d_{mI}} \tag{6}$$

where d_I is a function which measures the distance of the current sample knot (x,y) to knot (x_i,y_i), and the derivatives of r in different directions is defined as

$$\frac{\partial r}{\partial x} = \frac{1}{d_{mI}}\frac{(x-x_i)}{\sqrt{(x-x_i)^2+(y-y_i)^2}} \tag{7}$$

$$\frac{\partial r}{\partial y} = \frac{1}{d_{mI}}\frac{(y-y_i)}{\sqrt{(x-x_i)^2+(y-y_i)^2}} \tag{8}$$

The support size at a specified knot is calculated by $d_{mI} = d_{\max} \cdot C_I$, where $d_{\max}$ is a scaling parameter factor, typically 2.0-4.0 for a static analysis, and C_I is the distance which is used to guarantee a meaningful interpolation by searching for those nodes surrounding the current knot. The criterion of choosing an appropriate support for CSRBF is to make a trade-off ensuring both the non-singularity of the interpolation and a modest computational cost.

2.2.2 Parameterization of the level set function

Now, the discrete level set function can be approximated by centrally positioning CSRBFs at their pre-specified knots and at the same time distributing the bounded densities to these knots over the design domain. In this way, the values of the discrete level set function can be physically connected to material physical properties. The discrete level set function is expressed as

$$\Phi^{\mathrm{h}}(\mathrm{x},\mathrm{t}) = \boldsymbol{\Theta}^{\mathrm{T}}(\mathrm{x})\boldsymbol{\rho}(\mathrm{t}) = \sum_{i=1}^{N} \Theta_i(\mathrm{x})\rho_i(\mathrm{t}) \quad (0 < \rho_i \leq 1) \tag{9}$$

It is noted that $0 < \rho_i \leq 1$ is a regularized interval. The vector of the CSRBFs is given as

$$\boldsymbol{\Theta}(\mathrm{x}) = [\Theta_1(\mathrm{x}), \Theta_2(\mathrm{x}), ..., \Theta_{\mathrm{N}}(\mathrm{x})]_{N\times 1} \in \Re^{\mathrm{N}} \tag{10}$$

and the vector of the material densities at corresponding CSRBF knots

$$\boldsymbol{\rho} = [\rho_1, \rho_2, ..., \rho_N]_{N\times 1} \in \Re^{\mathrm{N}} \quad (0 < \rho_i \leq 1) \tag{11}$$

In doing so, the trial version of the level set function is uniquely determined in terms of the given values of the discrete level set function values at CSRBFs knots. Since the present interpolating scheme is performed under the assumption that all the knots are fixed in the design domain, leading to a separation of the space and time in the Hamilton-Jacobi PDEs. In this way, the radial basis functions are spatial functions only while the densities are temporal only. The level set model in Equation (1) is now described as

$$\boldsymbol{\Theta}^{\mathrm{T}}(\mathrm{x})\dot{\rho}(\mathrm{t}) - \mathrm{v_n}\left|(\nabla\boldsymbol{\Theta})^{\mathrm{T}}\boldsymbol{\rho}(\mathrm{t})\right| = 0 \tag{12}$$

where $\dot{\rho}(\mathrm{t})$ is the normal velocity field related to the derivatives of the material densities (general coefficients) with respect to the pseudo time, which is given as

$$\mathrm{v_n} = \frac{\boldsymbol{\Theta}^{\mathrm{T}}(\mathrm{x})}{|\nabla\Phi|}\dot{\rho}(\mathrm{t}), \text{ where } \dot{\rho}(\mathrm{t}) = \frac{d\boldsymbol{\rho}(\mathrm{t})}{d\mathrm{t}} \tag{13}$$

where

$$|\nabla\Phi| = \left[\left(\frac{\partial\boldsymbol{\Theta}^{\mathrm{T}}}{\partial\mathrm{x}}\boldsymbol{\rho}\right)^2 + \left(\frac{\partial\boldsymbol{\Theta}^{\mathrm{T}}}{\partial\mathrm{y}}\boldsymbol{\rho}\right)^2\right]^{1/2} \tag{14}$$

where

$$\frac{\partial \mathbf{\Theta}}{\partial \mathrm{x}} = \left[\frac{\partial \Theta_1}{\partial \mathrm{x}} \quad \ldots \quad \frac{\partial \Theta_N}{\partial \mathrm{x}}\right]^{\mathrm{T}} \tag{15}$$

$$\frac{\partial \mathbf{\Theta}}{\partial \mathrm{y}} = \left[\frac{\partial \Theta_1}{\partial \mathrm{y}} \quad \ldots \quad \frac{\partial \Theta_N}{\partial \mathrm{y}}\right]^{\mathrm{T}} \tag{16}$$

where $\partial\Theta_{\mathrm{i}}/\partial x$ and $\partial\Theta_{\mathrm{i}}/\partial y$ can be obtained according to Equations (4) and (5).

In the above equations, it can be found that the densities are explicitly time-dependent and all the time dependence of the level set model in Equation (9) is due to the density field. Initially (t = 0), the densities need to be distributed at all the nodes over the entire design domain. If the interpolation data Φ_{I} (I = 1,...,N) of the discrete level set values at these knots are pre-known, we have the following expression by letting $\Phi^{\mathrm{h}}(\mathbf{x}_{\mathrm{I}}) = \Phi_{\mathrm{I}}$. In numerical implementation, the densities (t = 0), a kind of regularized interpolation coefficients, can be obtained according to the interpolation matrix $\mathbf{A}$ that is theoretically invertible.

$$\underbrace{\boldsymbol{\rho}_{(t=0)}}_{N\times 1} = \underbrace{\mathbf{A}^{-1}}_{N\times N}\underbrace{\mathbf{\Phi}}_{N\times 1} \tag{17}$$

where

$$\mathbf{\Phi} = [\Phi_1, \Phi_2, ..., \Phi_N] \tag{18}$$

Hence, the densities at the initial time $\boldsymbol{\rho}_{(\mathrm{t}=0)}$ can be obtained according to the interpolation matrix $\mathbf{A}$ and the vector $\mathbf{\Phi}$ including the interpolation data of the initial level set surface. The interpolation matrix $\mathbf{A}$ can be expressed as follows according to the CSRBFs:

$$\mathbf{A} = \begin{bmatrix} \mathbf{\Theta}^{\mathrm{T}}(\mathbf{x}_1) \\ \mathbf{\Theta}^{\mathrm{T}}(\mathbf{x}_2) \\ \ldots \\ \mathbf{\Theta}^{\mathrm{T}}(\mathbf{x}_N) \end{bmatrix} = \begin{bmatrix} \Theta_1(\mathbf{x}_1) & \Theta_2(\mathbf{x}_1) & \ldots & \Theta_N(\mathbf{x}_1) \\ \Theta_1(\mathbf{x}_2) & \Theta_2(\mathbf{x}_2) & \ldots & \Theta_N(\mathbf{x}_2) \\ \ldots & \ldots & \ldots & \ldots \\ \Theta_1(\mathbf{x}_N) & \Theta_2(\mathbf{x}_N) & \ldots & \Theta_N(\mathbf{x}_N) \end{bmatrix} \tag{19}$$

After getting the initial density field vector $\boldsymbol{\rho}_{(\mathrm{t}=0)}$, the subsequent interpolations for Φ can be determined according to the updated density field $\boldsymbol{\rho}_{(\mathrm{t}>0)}$ spatially scattered at the CSRBF knots and the interpolation matrix $\mathbf{A}$ already obtained. Advancing the level set function in this study is thus equal to update density field $\boldsymbol{\rho}(\mathrm{t})$ (design variable vector) in time using appropriate design optimization algorithm. Equation (13) also indicates a natural velocity extension over the entire domain because the normal velocity vector $\mathbf{v}_{\mathrm{n}}$ are naturally applied to all CSRBF knots over the design domain rather than only the points around the front. As described below, this paper doesn't need to explicitly calculate vector $\mathbf{v}_{\mathrm{n}}$. The first derivative of $\boldsymbol{\rho}$ with respect to pseudo time t can be obtained via shape derivative analysis.

3 Shape derivative for design sensitivity analysis

The following structural mean compliance design is used for design sensitivity analysis because of its well-established theory [Bendsøe and Sigmund (2003)]. In this study, the linear elastic structure is considered only for the sake of numerical simplicity but without losing any generality.

$$\begin{aligned} &\underset{\Phi}{\text{Minimize}} : J(u,\Phi) = \int_D f(u,v)\mathbf{H}(\Phi)d\Omega \\ &\text{Subject to:} \begin{cases} G(\Phi) = \int_D \mathbf{H}(\Phi)d\Omega - V_0 \le 0 \\ 0 < \rho_{j,\min} \le \rho_j \le \rho_{j,\max} \\ \mathbf{a}(u,v,\Phi) = \mathbf{l}(v,\Phi), \;\; u|_{\Gamma_D} = u_0, \forall v \in \mathbf{U} \end{cases} \end{aligned} \tag{20}$$

where $f(u,v) = \boldsymbol{\varepsilon}_{ij}(u)\mathbf{D}_{ijkl}\boldsymbol{\varepsilon}_{kl}(v)/2$ is the structural mean compliance, and $\mathbf{D}$ is material elasticity tensor which can be obtained in terms of the point-wise densities at all CSRBF knots. ε is the strain field, and u is the displacement field. v is the virtual displacement field belonging to the space $\mathbf{U}$ spanned by the kinematically admissible set of displacements, and u_0 is the prescribed displacement on the admissible Dirichlet boundary Γ_D. The first inequality constraint is introduced to limit the allowable material usage, and V_0 is the prescribed volume. $\mathbf{H}(\Phi)$ is the Heaviside step function which serves as a characteristic function to uniformly indicates different parts in the design domain, and in practice a smoothed function is applied due to the consideration of differentiability. $\rho_{j,\min}$ and $\rho_{j,\max}$ are a pair of regularized lower and upper bounds to make the material density field practically meaningful. In practice, $\rho_{\min} = 0.0001$ and $\rho_{\max}$=1 are used to indicate two different material phases, and $\rho_{\min} = 0.0001$ denotes the void weakness material used to avoid numerical singularity in finite element process.

The state equation $\mathbf{a}(u,v,\Phi) = \mathbf{l}(v,\Phi)$ is written in weak variational form in terms of the energy bilinear functional $\mathbf{a}(u,v,\Phi)$ and the load linear form $\mathbf{l}(v,\Phi)$, which can be defined as

$$\mathbf{a}(u,v,\Phi) = \int_D \mathbf{c}(u,v)\mathbf{H}(\Phi)d\Omega = \int_D \underbrace{\boldsymbol{\varepsilon}_{ij}(u)\mathbf{D}_{ijkl}\boldsymbol{\varepsilon}_{kl}(v)}_{\mathbf{c}}\mathbf{H}(\Phi)d\Omega \tag{21}$$

$$\mathbf{l}(v,\Phi) = \int_D \mathbf{p}v\mathbf{H}(\Phi)d\Omega + \int_D \tau v\delta(\Phi)\left|\nabla\Phi\right|d\Omega \tag{22}$$

where $\mathbf{c}(u,v)$=$\boldsymbol{\varepsilon}_{ij}(u)\mathbf{D}_{ijkl}\boldsymbol{\varepsilon}_{kl}(v)$ is the strain energy density. $\mathbf{p}$ is the body force and τ is the boundary traction vector. $\delta(\Phi)$ is the Dirac function, the partial derivative of $\mathbf{H}(\Phi)$.

3.1 Shape derivative analysis

In this study, the shape derivative analysis is used to perform the design sensitivities. The material derivative is included in the process of the shape derivative analysis. More details for the shape derivative and the material derivative, the readers can refer to the related literatures [e.g. Sokolowski and Zolesio (1992); Choi and Kim (2005)].

First, the Lagrangian method is applied to convert the original constrained optimization problem to an unconstrained one as follows:

$$L(u,\Phi) = J(u,\Phi) + \lambda\,[\mathbf{l}(v,\Phi) - \mathbf{a}(u,v,\Phi)] + \Lambda\left[\int_D \mathbf{H}(\Phi)d\Omega - V_0\right] \tag{23}$$

where λ is introduced as the Lagrange multiplier relevant to the state equation, which can be dropped from the Lagrangian by considering the linearity of the admissible space, and Λ is the Lagrange multiplier of the volume constraint. So the shape derivative of L can be obtained as

$$\frac{\partial L(u,\Phi)}{\partial t} = \int_{\partial D} \beta(u,v,\Phi)\mathbf{H}(\Phi)(\mathbf{v}(x)\cdot\mathbf{n})d\Omega \tag{24}$$

with the **shape gradient density** defined by

$$\beta(u,v,\Phi) = f(u,v) - \boldsymbol{\varepsilon}_{ij}(u)\mathbf{D}_{ijkl}\boldsymbol{\varepsilon}_{kl}(v) + [pv + \nabla(\tau v)\cdot\mathbf{n} + \kappa(\tau v)] + \Lambda \tag{25}$$

where $\kappa = div\mathbf{n} = \nabla\cdot\mathbf{n} = \nabla\cdot(-\nabla\Phi/|\nabla\Phi|)$ is the mean curvature in two-dimensions. Most standard level set methods directly let $\mathbf{v}_n = -\beta$ to ensure a steepest descent of the objective function [Wang, Wang and Guo (2003); Allaire, Jouve and Toader (2004)]. However, it is well known that the steepest descent method is a classic gradient method which can only allow a fast descent locally rather than globally. Hence, the more efficient optimization algorithms are in demands in order to ensure the decrease of the objective function under the constraint(s).

It is noted that the shape derivative of Lagrangian function agrees with the derivative of the objective functional when all the constraints are satisfied. The optimal criteria of the structure is related to the stationary point of the Lagrangian by letting $\delta L = 0$, respectively denoting that $\partial(L(u,\Phi))/\partial v = 0$ can lead to the state equation, $\partial(L(u,\Phi))/\partial u = 0$ can be applied to find the adjoint equation and $\partial(L(u,\Phi))/\partial\Lambda = 0$ is used to express the equation of the inequality condition. The strong formulation of the optimality criteria can be found via $\partial(L(u,\Phi))/\partial\Phi = 0$. So the necessary condition for an optimal configuration can be stated as

$$f(u,v) - \boldsymbol{\varepsilon}_{ij}(u)\mathbf{D}_{ijkl}\varepsilon_{kl}(v) + [pv + \nabla(\tau v)\cdot\mathbf{n} + \kappa(\tau v)] = -\Lambda \tag{26}$$

which shows that the **shape gradient density** will be close to constant at the free design boundary of the optimal structural configuration.

3.1.1 Design sensitivities

Recalling the normal velocity field $\mathbf{v}_{\mathrm{n}}$ defined in Equation (13) and substituting it into Equation (24), the shape derivative of L is thus given as follows assuming a relationship $\beta = \vartheta + \Lambda$:

$$\frac{\partial L(u,\Phi)}{\partial t} = \sum_{i=1}^{N}\left(\int_{\partial D}\vartheta(u)\frac{\Theta_i(\mathbf{x})}{\left|(\nabla\boldsymbol{\Theta})^{\mathrm{T}}\boldsymbol{\rho}(\mathrm{t})\right|}d\Gamma\right)\dot{\rho}(t) + \Lambda\sum_{i=1}^{N}\left(\int_{\partial D}\frac{\Theta_i(\mathbf{x})}{\left|(\nabla\boldsymbol{\Theta})^{\mathrm{T}}\boldsymbol{\rho}(\mathrm{t})\right|}d\Gamma\right)\dot{\rho}(t) \quad (27)$$

On the other hand, the shape derivative of L can be expressed as follows via the chain rule

$$\frac{\partial L(u,\Phi)}{\partial t} = \sum_{i=1}^{N}\left(\frac{\partial J(u,\Phi)}{\partial\rho_i(t)}\right)\dot{\rho}(t) + \Lambda\sum_{i=1}^{N}\left(\frac{\partial G(u,\Phi)}{\partial\rho_i(t)}\right)\dot{\rho}(t) \quad (28)$$

Comparing the terms in Equations (27) and (28), we can get the design sensitivities as

$$\frac{\partial J(u,\Phi)}{\partial\rho_i(t)} = \int_{\partial D}\left(\vartheta(u)\frac{\Theta_i(\mathbf{x})}{\left|(\nabla\boldsymbol{\Theta})^{\mathrm{T}}\boldsymbol{\rho}(\mathrm{t})\right|}\right)d\Gamma \quad (29)$$

$$\frac{\partial G(u,\Phi)}{\partial\rho_i(t)} = \int_{\partial D}\left(\frac{\Theta_i(\mathbf{x})}{\left|(\nabla\boldsymbol{\Theta})^{\mathrm{T}}\boldsymbol{\rho}(\mathrm{t})\right|}\right)d\Gamma \quad (30)$$

By far, we have obtained the design sensitivities of the objective function and the constraint with respect to the design variables ρ_i $(i = 1,2,...N)$ at CSRBF knots over the design domain. To improve efficiency in numerical implementation, the design sensitivity in Equations (29) and (30) can be calculated using a more efficient volume integration scheme. Considering the relation $d\Gamma = \delta(\Phi)\left|\nabla\Phi\right|d\Omega$, we have

$$\frac{\partial J(u,\Phi)}{\partial\rho_i} = \int_D\left\{\vartheta(u)\Theta_i(\mathbf{x})\delta_\varepsilon(\Phi)\right\}d\Omega \quad (31)$$

$$\frac{\partial V(\Phi)}{\partial\rho_i} = \int_D\left\{\Theta_i(\mathbf{x})\delta_\varepsilon(\Phi)\right\}d\Omega \quad (32)$$

where δ_ε is a regularized version of the Dirac function given as follows:

$$\delta_\varepsilon(\Phi) = \frac{1}{\pi\varepsilon \cdot \left(1+\left(\frac{\Phi}{\varepsilon}\right)^2\right)} \tag{33}$$

Here ε is a real positive constant, and it is usually chosen as 2-4 times as the mesh size in terms of numerical experiences [Luo, Tong and Wang (2008)]. Once getting the design sensitivities for the objective function and the constraint, the rest is just a question of applying optimization algorithms, e.g. MMA method [Svanberg (1987)], to update the design variables in time, so as to implement structural shape and topology changes.

4 Finite element approximation with nodal material densities

This study uses CSRBFs and nodal material densities to approximate the level set surface, and then the densities is applied to interpolate the practical material properties using the standard finite element shape functions. So the nodal densities not only act as the interpolation data to propagate the level set surface, but also serve as the design variables to represent material properties. So the property of non-negative and value-bounded is of significance in structural topology optimization in order to uniformly indicate the solid and void material points in the design domain. Here, to some extent, we can see that the concept in this Section is similar to that in SIMP, as in both cases the regularized material densities are used as design variables to interpolate practical material properties. One difference is that the proposed method is based on point-wise rather than element-wise design variables as that in SIMP approaches. Furthermore, no 'power-law' is required to penalize the intermediate densities in this work.

In numerical implementation, the discontinuities crossing boundary elements in the finite element approximation can be well approximated without remeshing for moving discontinuities. The strain for those elements by far can be modeled via several methods, for instance, the popular "ersatz material" scheme [Alliare, Jouve and Toader (2004)]. While in this study the densities serve as the design variables to be updated, and a new numerical scheme for calculating nodal strain will be presented. For the standard quadrilateral elements, the element density, Young's modulus and elastic constant can be represented using nodal interpolation as follows, respectively:

$$\rho_e = \sum_{I=1}^{n_{nod}} N_I \rho_I, (I = 1,2,...,n_{nod}) \tag{34}$$

where ρ_{I} are material densities at elemental nodes, E_0 and D_0 are Young's modulus and elasticity constant for the solid material. N_{I} is the Lagrangian shape function

in the standard finite element method. The above two equations are based on the quadrilateral elements with the nodal number $n_{nod} = 4$, but it is straightforward to higher-order elements or non-quadrilateral elements. Here, we represent the practical element density, stiffness and elasticity constant according to the point-wise material densities that are the design variables.

For the element stiffness matrix $\mathbf{K}_e$

$$\mathbf{K}_e = \int_{\Omega_e} \mathbf{B}_e^T \mathbf{D}_e \mathbf{B}_e dV \tag{35}$$

which can be calculated in terms of the Equation (35) with numerical Gauss integration:

$$\mathbf{K}_e(x_{gp}) = \sum_{gp=1}^{n_{gp}} \left[hB_e^T(x_{gp}) \left(\sum_{I=1}^{4} N_I(x_{gp})(\rho_I D_0) \right) B_e(x_{gp}) J(x_{gp}) w_{gp} \right] \tag{36}$$

With two dimensional 2-point Gauss quadrature for the integration, we have

$$\mathbf{K}_e(x_{gp}) = \sum_{i=1}^{2} \sum_{j=1}^{2} \left[hB_e^T(s_i,t_j) \left(\sum_{I=1}^{4} N_I(s_i,t_j)(\rho_I D_0) \right) B_e(s_i,t_j) J(s_i,t_j) w_i w_j \right] \tag{37}$$

where J is Jacobi determinant, $s_i,t_j = \pm 0.5773$, and $w_i,w_j = 1,1$ ($i = 1,2$, $j = 1,2$). "gp" represents the number of gauss points in the e^{th} element, x_{gp} represent the gauss integration point, w is the corresponding weighting factors. **B** is the usual displacement-strain matrix and **D** is the elastic matrix computed using the material properties at the point x_{gp}.

Another aspect is to construct a material density field with global smoothness over the entire design space according to nodal design variables. With this scheme, the density field is expected to include not only the contribution of the design variables of those nodes within one element but also the nodes belonging to the neighboring elements within an influential support. In this work, a weighting regularization scheme with a Wendland C4 CSRBF integral kernel [Wendland (2005)] is proposed to create a smooth density field:

$$\bar{\rho}_I(r) = \left(\sum_{J=1}^{n_H} \Upsilon_{J,I}(r) \boldsymbol{\rho}_I \right) / \sum_{J=1}^{n_H} \Upsilon_{J,I}(r), \text{where}$$

$$\Upsilon_{J,I}(r) = \frac{\Theta(r(x_I,x_J))}{\sum_{I=1}^{n_H} \Theta(r(x_I,x_J))} \tag{38}$$

where $\boldsymbol{\rho}$ and $\bar{\rho}$ are the original and smoothed material density fields, respectively. n_H is the number of the nodes that is within the support radius r of the I^{th} point. Υ

is the convolution operator defined by an integral kernel Θ. We can find that the convolution operator Υ is just a special case of the Shepard function with zero-order of consistency. So the material density at a specific computational point is actually determined by the nodal densities inside the influential support. Mesh refinement can increase the density points within the compact support radius, leading to the improvement of the computational accuracy. Hence, in interpolating the level set function during numerical implementation, the design variable vector $\boldsymbol{\rho}$ will be replaced by the smoothed density field $\bar{\rho}$ via a Shepard function-based convolution scheme, in order to practically enhance the smoothness of the parametric level set function.

5 Numerical examples

In this section, two benchmark numerical examples, the cantilever and MBB beams, are used to demonstrate the effectiveness of the present level set method. The level set function is initially embedded as a signed distance function, but no further reinitialization is applied in the rest of iterations. The point values of the material densities are positioned at CSRBF knots which are not necessarily but supposed to be consistent with element nodes for simplicity. For the "artificial" material model, Young's modulus for solid material is 1, for weak material is 0.0001, and Poisson's ratio is 0.3. In the topology optimization, the units for the artificial material can be defined flexibly but all the units are required to be uniformly during the design optimization.

5.1 Cantilever beam

Figure 1 is the design domain of the cantilever beam with L=50. The left side of the domain is fixed as the Dirichlet boundary while the right side is treated as a non-homogenous Neumann boundary with a concentrated force F=1 vertically applied at the center point. The objective function is to minimize the mean compliance, and the constraint is to limit the allowable material usage no more than 50%. The design domain is discretized with 100×50 quadrilateral elements. As shown in Figure 2, the CSRBF knots and elemental nodes are uniformly scattered at the same set of points, where the point-wise densities or the design variables are located.

The shape and topology optimization is converged after 450 iterations, and the overall structural mean compliance is minimized from 239.7314 to 60.1639. Figure 3 shows the discrete plots of the nodal densities at different design stages. The set of densities are used to interpolate the level set function with the CSRBFs. At the same time, they serve as the design variables of the parametric optimization to propagate the discrete level set function. The contours of the design variables are displayed in Figure 4 that shows the design gradually moves towards the lower limit

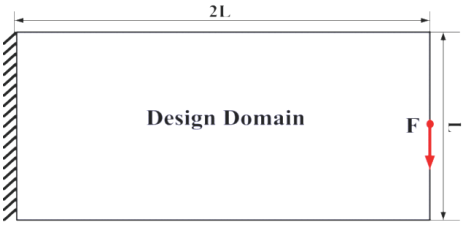

Figure 1: Design domain of the cantilever beam (left)

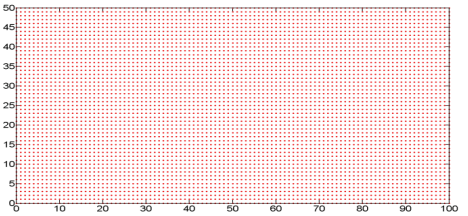

Figure 2: CSRBF knots or FE nodes in the design domain (right)

$\rho_{\min} = 0.0001$ (weak material phase) and upper limit $\rho_{\max} = 1$ (solid material phase) during the optimization. So we can say that the topology optimization is actually an iterative process to re-distribute a number of density points in the design domain in terms of the design sensitivities until the design approaches toward a so-called "0-1" distribution.

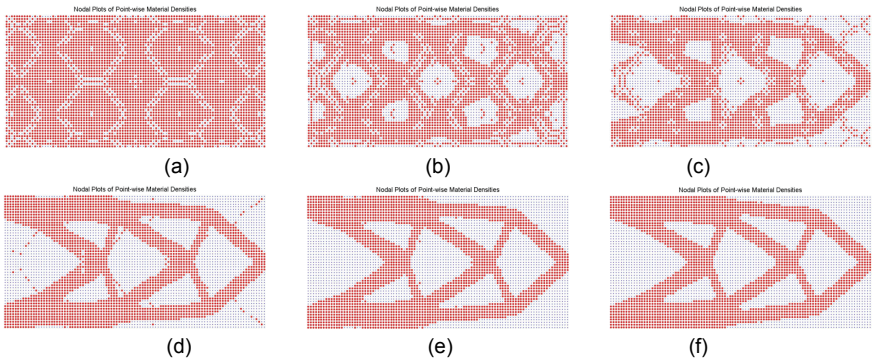

Figure 3: Topology plots of point-wise nodal material densities

Figures 5 and 6 showcase the level-set based topology contours and the corresponding level set surfaces during different design stages. It can be found that the material densities and the CSRBFs can be employed to approximate the level set function, and so make the level set interpolant own some definite physical meanings. In this way, on one hand, the favorable advantages of the level set method are well maintained, such as the concise interface and smooth boundary, merging and nucleating new holes to enable shape fidelities and topological flexibilities. Further the initial level set surface has a simple topology but it can implement complicated topology changes. On the other hand, one attraction of this method is the connection

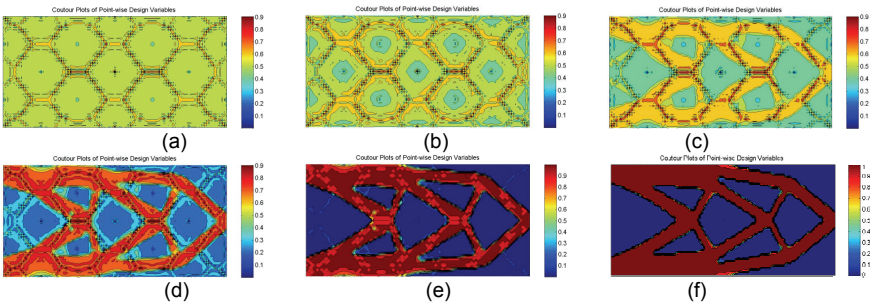

Figure 4: Contour plots of point-wise nodal design variables

of the conventional level-set representation with efficient optimization algorithms via physically meaningful level set interpolation which is of significance in evaluating material properties of mechanics. Figure 7 shows the contour plots of the discrete values of the parametric level set function. In Figure 7, we can also see that the level set function values are non-negative and with an upper bound due to the range-bounded nodal densities ($0 < \boldsymbol{\rho} \leq 1$). However, in different steps the upper bounds of the level set function are different due to the interpolation of the CSRBFs with the different nodal densities in time. So, it can be seen that the proposed level set method can implicitly represent boundary with a set of constant level sets which can adaptively adjust their values in different steps.

Figure 8 displays curves of the objective function and the volume constraint over the iterations. It can be seen that the first 10 iterations are mainly used to push material volume back to satisfy the constraint. Then the subsequent 90 iterations (roughly) are used to implement structural topology changes and the rest 350 iterations are consumed to achieve the shape variation. It is noted that the 350 iterations are worthwhile in satisfying the optimal criteria until a uniform distribution of the strain energy achieved in the structure or the normal velocity field is close to zero at the design boundary. Hence, we can see that the topology process aims to achieve an overall material distribution layout while the following shape optimization endeavors to improve the specified structural performance locally. Furthermore, the constraint curve shows that the proposed method is well mass conservative, compared to most conventional level set methods. For this benchmark example, it can be found the final design is similar to that reported in the literature [e.g. Wang, Wang and Guo (2003); Allaire, Jouve and Toader (2004)].

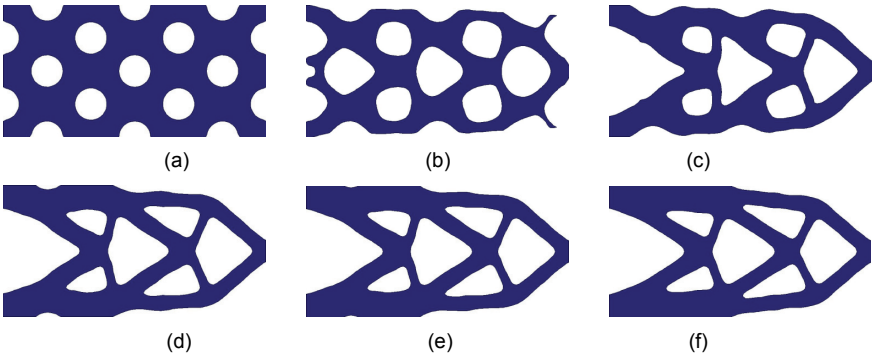

Figure 5: Topology plots of level-set contours

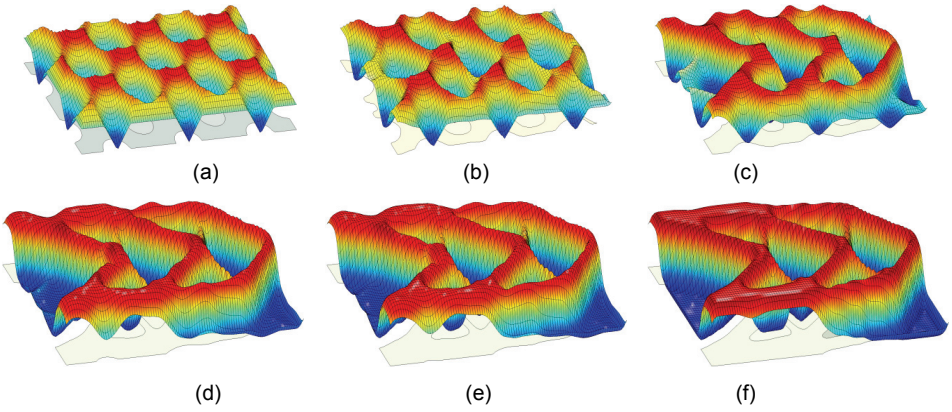

Figure 6: Propagation of the discrete level set surface

5.2 MBB beam

In Figure 9, a vertically force F=1 is applied to at the center point of the upper side of the MBB structure. The bottom-left corner is fixed and the bottom-right corner is simply supported as a roller. The artificial material properties are defined as: Young's modulus for solid material phase is 1 and for the weak material phase is 0.0001, and both materials have Poisson's ratio 0.3. The allowed material usage is limited to 50%. The beam length and width size ratio is 6:1 with a width of L=30. The design domain is discretized with 180×30=5400 quadrilateral finite elements, and the elemental nodes are scattered inside the design domain as Figure 10.

The final design is obtained after 537 iterations, with the overall strain energy be-

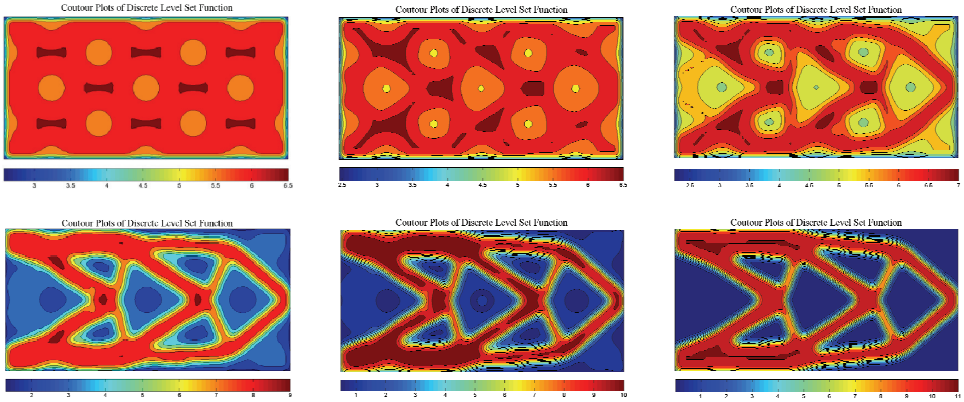

Figure 7: Contour plots of the discrete level set function values

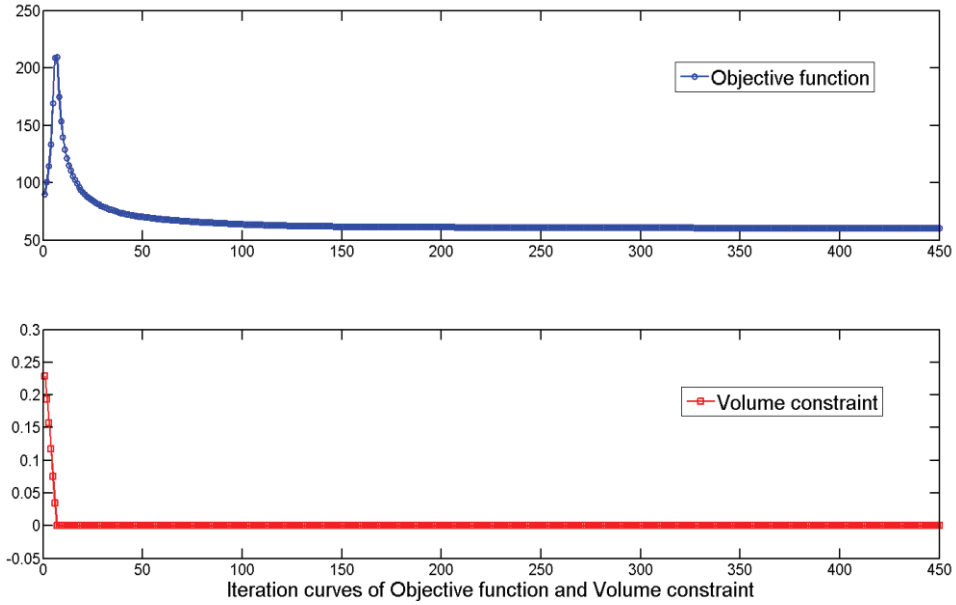

Figure 8: Curves of objective function and volume constraint

ing minimized from 334.8343 to 92.4188. Figure 11 shows the discrete plots of the point-wise densities, while the Figure 12 displays the continuous contour plots of the nodal densities. We can see that the regularized density field is gradually converges to the lower and upper bounds of the design variables (0.0001 and 1) which are used to indicate the weakness and solid material phases in the design

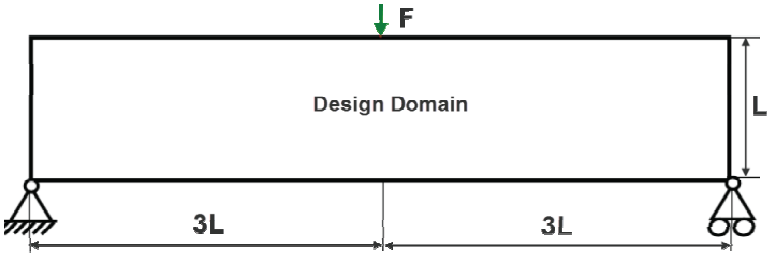

Figure 9: Design domain for the Michell-type structure

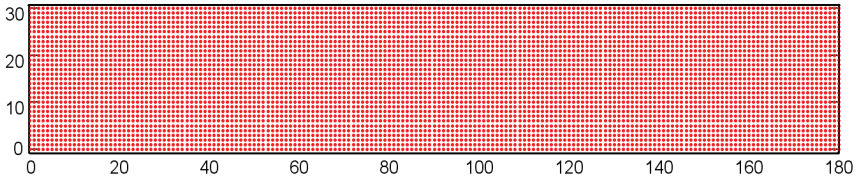

Figure 10: FE (CSRBFs) nodes scatter in the design domain

domain, respectively. The design boundary is embedded into constant level set (Φ_i=Constant) of the level set function Φ. The level set topology contours at Φ Φ_i=C_i and their corresponding level set surfaces are respectively given in Figure 13 and Figure 14. It can be found that the optimal design can be obtained via shape fidelity and topological changes by deleting existing holes and adding new holes inside the design domain.

Compared with the most standard level set methods with explicit time schemes, the present nodal-density based level set method is time-stable for all the CSRBFs knots with any practical moving limit, because it is easily to understand that the moving limit in the MMA algorithm doesn't limit by the CFL condition [Sethian (1999)]. In numerical implementation, a little bit experience is needed in selecting the appropriate moving limit for MMA optimizer, because an impractically large move limit may delete those sub-structures including the possible optimal topology configuration during initial iterations, while a too small value will unnecessarily make computation expensive. Figure 15 shows the contour plots of the discrete level set function values, which denotes that the parametric level set function at all CSRBF knots are larger than zero and bounded with upper limits. From Figure 16, it can be seen that the present level set is mass conservative, and shape and topology variations can be implemented flexibly in the same design domain. The present level set method can lead to the optimal design similar to the widely ac-

cepted examples reported in the literatures [e.g. Sigmund (2001); Wang, Wang and Guo (2003); Allaire, Jouve and Toader (2004); Luo, Tong and Wang (2008)].

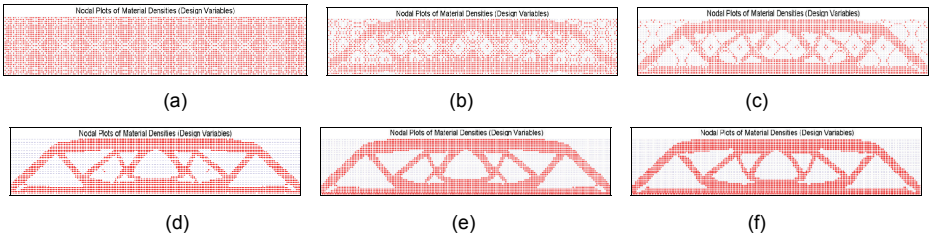

Figure 11: Nodal plots of point-wise material densities

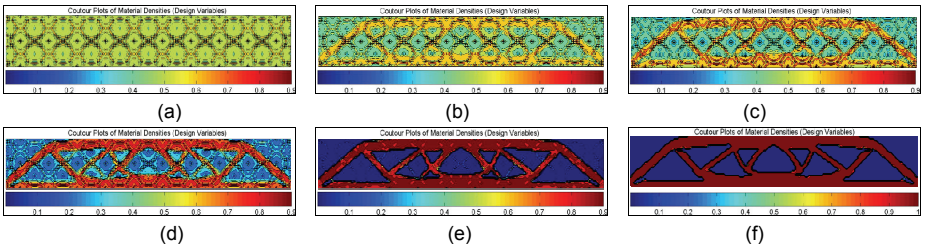

Figure 12: Contour plots of nodal material densities

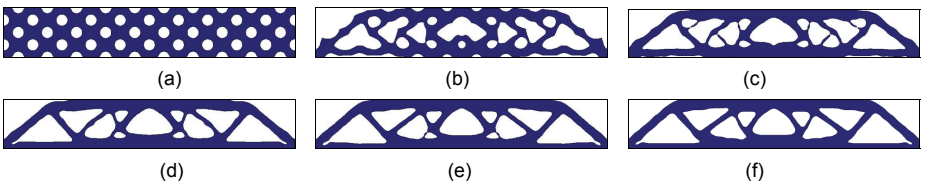

Figure 13: Topology plots of level-set contour

In this Section, two typical numerical examples (cantilever and MBB beams) have been used to showcase the effectiveness of the proposed level set method. From the final results, we can see that the nodal density-based level set method can obtain optimal designs similar to the widely reported results in most conventional topology optimization methods. Hence, we can implicitly define design boundary at

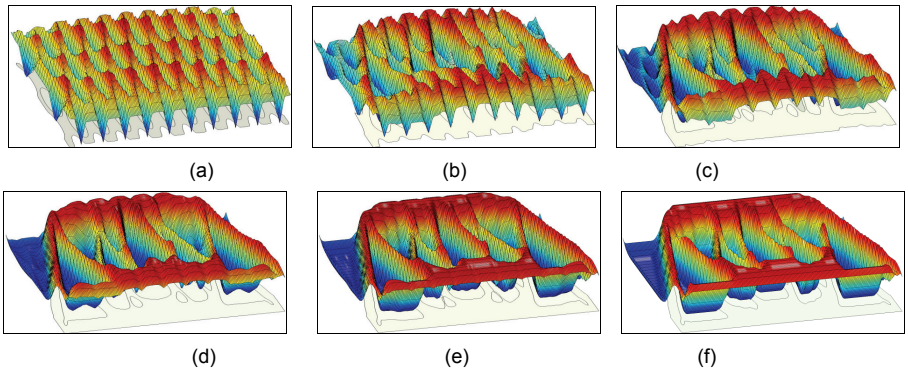

Figure 14: Level set surface with CSRBFs and nodal point-wise densities

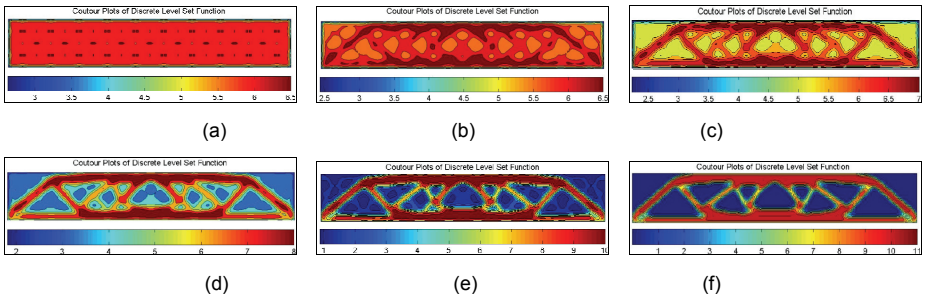

Figure 15: Contour plots of discrete level set function values

non-zero level sets of the level set function to cater for constructing a physically meaningful level set function. In this way, both the level set function propagation and the shape derivative analysis are based on the underlying material properties that have definite physical meanings. To compare numerical details for different topology optimization methods, the readers can refer to the related references for further information. It is straightforward to extend the proposed method to more advanced topology design problems.

6 Conclusions

This study has proposed a physically meaningful level set method for structural shape and topology optimization based on a nodal density interpolation scheme using CSRBFs. The design boundary is implicitly embedded into a higher-dimensional scalar function as non-zero level sets. The CSRBFs and point-wise nodal densities

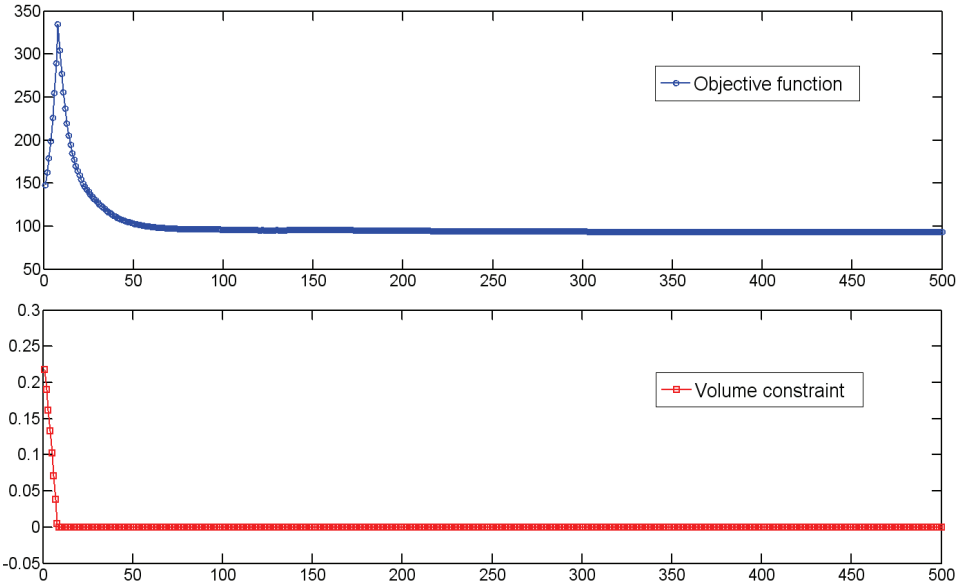

Figure 16: Curves of objective function and volume constraint

at a uniformly defined set of points (nodes, or knots) are used to interpolate the level set function, leading to a smooth level set function with definite physical meanings. The original more difficult shape and topology optimization driven by the Hamilton-Jacobi PDE is fully parameterized into a relatively easier size optimization of the densities. The set of the CSRBFs is not only used to parameterize the level set function, but also applied to construct an improved density field with enhanced smoothness. The density field has triple functions to (1) act as the scattered data to interpolate the discrete level set function, (2) serve as the design variables to propagate the level set function in time, and (3) approximate the practical material properties. The motion of design boundary is thus equivalent to transporting the level set function via an iterative numerical process by updating the discrete level set surface. Two benchmark examples in the context of structural mean compliance design are used to demonstrate the effectiveness of the proposed method. It can be seen that the present level set method not only possesses the merits of the implicit free boundary representation schemes but also can avoid numerical difficulties in the standard level set method.

Acknowledgement: This research work is partially supported by Chancellor's Research Fellowship 2011 (University of Technology, Sydney), National Natural-

Science-Foundation of China, NSFC (51105229, 51175197), and Open Research Foundation (DMETKF2010004) of "State Key Lab. of Digital Manufacturing Equipment & Technology", Huazhong University of Science & Technology, China. The authors thank Prof. Krister Svanberg for providing his MMA codes.

References

Allaire, G., Jouve, F., Toader, A.M. (2004): Structural optimization using sensitivity analysis and a level-set method, *Journal of Computational Physics*, vol. 194, pp. 363-393.

Belytschko, T., Xiao, S.P., Parimi, C. (2003): Topology optimization with implicitly function and regularization, *International Journal for Numerical Method in Engineering*, vol. 57, pp. 1177-1196.

Bendsøe, M.P., Kikuchi, N. (1988): Generating optimal topology in structural design using a homogenization method, *Computer Methods in Applied Mechanics and Engineering*, vol. 71, pp. 197-224.

Bendsøe, M.P., Sigmund, O. (1999): Material interpolation schemes in topology optimization, *Archive of Applied Mechanics*, vol. 69, pp. 635-654.

Bendsøe, M.P., Sigmund, O. (2003): Topology optimization: Theory, Methods, and Applications, Springer, Berlin Heidelberg.

Buhmann, M.D. (2004): Radial Basis Functions: Theory and Implementations, Cambridge Monographs on Applied and Computational Mathematics, Vol. 12, Cambridge University Press, New York.

Choi, K.K., Kim, N.H. (2005): Structural sensitivity analysis and optimization ¢ñ-Linear systems, Springer, New York, USA.

Du, Y., Luo, Z., Tian, Q. and Chen, L. (2009): Topology optimization for thermo-mechanical compliant actuators using meshfree methods, *Engineering Optimization*, vol. 41, pp. 753-772.

Haber, E. (2004): A multilevel, level-set method for optimizing eigenvalues in shape design problems, *Journal of Computational Physics*, vol. 198, pp. 518-534.

Kang, Z., Wang, Y.Q. (2011): Structural topology optimization based on non-local Shepard interpolation of density field, *Computer Methods in Applied Mechanics and Engineering*, vol. 200; pp. 3515-3525.

Kang, Z., Wang, Y.Q. (2012): A nodal variable method of structural topology optimization based on Shepard interpolant, *International Journal for Numerical Methods in Engineering*, in press, DOI:10.1002/nme.3321.

Li, S., Atluri, S.N., (2008): The MLPG mixed collocation method for material orientation and topology optimization of anisotropic solids and structures, *CMES:*

Computer Modeling in Engineering & Sciences, vol. 30, pp. 37-56.

Luo, Z., Tong, L., Wang, M.Y. (2008): Shape and topology optimization of compliant mechanisms using a parameterization level set method, *Journal of Computational Physics*, vol. 227, pp. 680-705.

Luo, Z., Tong, L., Luo, J., Wang, M.Y. (2009): Design of piezoelectric actuators using a multiphase level set method of piecewise constants, *Journal of Computational Physics*, vol. 228, pp. 2643-2659.

Osher, S., Sethian, J.A. (1988): Front propagating with curvature dependent speed: Algorithms based on Hamilton-Jacobi formulations, *Journal of Computational Physics*, vol. 78, pp. 12-49.

Osher, S., Santosa, F. (2001): Level-set methods for optimization problem involving geometry and constraints: I. Frequencies of a two-density inhomogeneous drum, *Journal of Computational Physics*, vol. 171, pp. 272-288.

Osher, S., Fedkiw, R.P. (2002): Level set methods and dynamic implicit surface. Springer, New York.

Rozvany, G.I.N. (2009): A critical review of established methods of structural topology optimization, *Structural and Multidisciplinary Optimization*, vol. 37, pp. 217-237.

Sethian, J.A. (1999): Level set methods and fast marching methods: Evolving interfaces in computational geometry, fluid mechanics, computer version and material science, Cambridge University Press, Cambridge, UK.

Sethian, J.A., Wiegmann, A. (2000): Structural boundary design via level set and immersed interface methods, *Journal of Computational Physics*, vol. 163, pp. 489-528.

Sigmund, O. (2001): A 99 line topology optimization code written in Matlab, *Structural and Multidisciplinary Optimization*, vol. 21, pp. 120-127.

Sokolowski, J., Zolesio, J.P. (1992): Introduction to shape optimization: Shape sensitivity analysis. Berlin: Springer.

Svanberg, K. (1987): The method of moving asymptotes: a new method for structural optimization, *International Journal for Numerical Method in Engineering*, vol. 24, pp. 359-373.

Tai, X.C. Li, H.W. (2007): A piecewise constant level set method for elliptic inverse problems, *Applied Numerical Mathematics*, vol. 57, pp. 686-696.

Wang, M.Y., Wang, X.M., Guo, D.M. (2003): A level set method for structural topology optimization, *Computer Methods in Applied Mechanics and Engineering*, vol. 192, pp. 227-224.

Wendland, H. (2005): Computational aspects of radial basis function approximation, in K. Jetter et al. (eds.), Topics in Multivariate Approximation and Interpolation. Elsevier B.V., 231-256.

Yamada, T., Izui, K., Nishiwaki, S., Takezawa, A. (2010a): A topology optimization method based on the level set method incorporating a fictitious interface energy, *Computer Methods in Applied Mechanics and Engineering*, vol. 199, pp. 2876-2891.

Yamasaki, S., Nishiwaki, S., Yamada, T., Izui, K., Yoshimura, M. (2010b): A structural optimization method based on the level set method using a new geometry-based re-Initialization scheme, *International Journal for Numerical Methods in Engineering*, vol. 83, pp. 1580-1624.

Zheng, J., Long, S.Y., Xiong, Y., Li, G.Y., (2008): A topology optimization design for the continuum structure based on the meshless numerical technique, *CMES: Computer Modeling in Engineering & Sciences*, vol. 29, pp. 137-154.

Zhou, M., Rozvany, G.I.N. (1991): The COC algorithm, Part II: topological, geometry and generalized shape optimization, *Computer Methods in Applied Mechanics and Engineering*, vol. 89, pp. 197-224.